ERRATA

Spherical nanoindentations and kink bands in Ti$_3$SiC$_2$

A. Murugaiah, M.W. Barsoum, S.R. Kalidindi, and T. Zhen
Department of Materials Science and Engineering, Drexel University, Philadelphia, PA 19104

We report on load versus depth-of-indentation response of Ti$_3$SiC$_2$ surfaces loaded with a 13.5 μm spherical tipped diamond indenter up to loads of 500 mN. Using orientation imaging microscopy, two groups of crystals were identified; one in which the basal planes were parallel to, and the other normal to, the surface. When the load-penetration depth curves were converted to stress-strain curves the following was apparent: when the surfaces were loaded normal to the c axis, the response at the lowest loads was linear elastic—well described by a modulus of 320 GPa—followed by a clear yield point at approximately 4.5 GPa. And while the first cycle was slightly open, the next 4 on the same location were significantly harder, almost indistinguishable, and fully reversible. At the highest loads (500 mN) pop-ins due to delaminations between basal planes were observed. When pop-ins were not observed the indentations, for the most part, left no trace. When the load was applied parallel to the c axis, the initial response was again linear elastic (modulus of 320 GPa) followed by a yield point of approximately 4 GPa. Here again significant hardening was observed between the first and subsequent cycles. Each cycle resulted in some strain, but no concomitant increase in yield points. This orientation was even more damage tolerant than the orthogonal direction. This response was attributed to the formation of incipient kink bands that lead to the formation of regular kink bands. Remarkably, these dislocation-based mechanisms allow repeated loading of Ti$_3$SiC$_2$ without damage, while dissipating significant amounts of energy per unit volume, W$_d$, during each cycle. The values of W$_d$ measured herein were in excellent agreement with corresponding measurements in simple compression tests reported earlier, confirming that the same mechanisms continue to operate even at the high (≈9 GPa) stress levels typical of the indentation experiments.

I. INTRODUCTION

The carbide Ti$_3$SiC$_2$ is a hexagonal layered compound belonging to a family of over 50 ternary carbides and nitrides with the general formula M$_{n+1}$AX$_n$, where n = 1 to 3, M is an early transition metal, A is an A-group (mostly IIIA and IVA) element, and X is C and/or N[1]. These compounds—best described as thermodynamically stable nanolaminates—possess an unusual combination of properties.[1]

The most studied, and best understood, to date is Ti$_3$SiC$_2$. It has the same density as Ti, but is almost three times as stiff and yet is readily machinable.[1–3] It is a better electrical and thermal conductor than Ti metal[3]; highly resistant to damage,[4,5] thermal shock,[3,4] fatigue,[6]

and creep.[7] It exhibits an increasing R-curve behavior,[6] with toughness values as high as 16 MPa·√m.

It is now fairly well-established that the Vickers microhardness values in Ti$_3$SiC$_2$ decrease with increasing loads down to a plateau value.[2,3,5,8,9] Furthermore, it is not possible to induce cracking from the corners of Vickers indentations even at loads of 500 N.[2,3,5] Diffuse microcracking, delamination, crack deflection, grain push-out, grain pull-out and the buckling of individual grains have all been identified as energy absorbing mechanisms.[5] Of special interest to this work is the work of Low et al.,[8] who showed that Hertzian indentation stress–strain response deviated strongly from linearity beyond a well-defined maximum, with pronounced strain–softening, indicating exceptional deformability in this otherwise stiff ceramic. Surface and subsurface ceramographic observations revealed extensive quasi-plastic microdamage zones at the contact sites. These

damage zones were made up of multiple intragrain slip and intergrain shear failures, with attendant micro-fracture at high strains. No ring cracks or other macro-scopic cracks were observed on, or below, the indented surfaces.

The unique characteristics of the mechanical response of Ti$_3$SiC$_2$ described above are directly attributable to the following facts: (i) basal slip, and only basal slip, is operative[10–13]; (ii) because of their high c/a ratios, twinning is unlikely, and has never been observed. Instead, deformation occurs by a combination of glide and kink band formation within individual grains,[10–13] and (iii) because they are confined to the basal planes, dislocations arrange themselves either in arrays (pile-ups) on the same slip plane, or in walls (tilt boundaries) normal to the arrays.[11,12] Dislocation interactions, other than orthogonal, are difficult and unlikely to occur, which allows them to move back and forth reversibly and extensively.

Most recently, we have shown that macroscopic poly-crystalline Ti$_3$SiC$_2$ cylinders can be compressed, at room temperature, to stresses of up to 1 GPa, and fully recover upon the removal of the load, while dissipating approxi-mately 25% of the mechanical energy.[14] The stress–strain curves at room temperature outline fully reversible, reproducible, rate-independent, closed hysteresis loops that are strongly influenced by grain size with the energy dissipated being significantly larger in the coarse-grained material. The loss factors for Ti$_3$SiC$_2$ are higher than most woods and comparable to polypropylene and nylon. Furthermore, the energy dissipated per cycle, W_d, was found to scale with the square of the applied stress, σ. In one case, a sample was cycled 100 times to 700 MPa, with no apparent changes in the shape or size of the loops. These observations were attributed to the forma-tion and annihilation of fully reversible incipient kink bands, or IKBs. IKBs are composed of near parallel dis-location walls of opposite polarity that remain attached and are thus attracted to each other. Removal of the load allows the walls to collapse and the IKB to be totally eliminated. At temperatures higher than 1000 °C, the stress–strain loops are open and the response becomes strain-rate dependent. However, cyclic hardening was observed at 1200 °C, for both fine and coarse-grained samples. At higher temperatures, the IKBs dissociate into mobile walls that in turn coalesce to form regular kink bands (KBs) that are no longer reversible.[14]

The purpose of this work is twofold. First, to study the response of Ti$_3$SiC$_2$ at high stresses (significantly above the 1 GPa stress imposed in the simple compression tests[14]) to explore if W_d continues to increase with in-creasing stresses. For this purpose, we decided to con-duct nanoindentation experiments using a spherical nanoindenter, where the stress levels under the indenter were of the order of 5–10 GPa. Second, we examined the influence of crystal lattice orientation on the mechanical response and deformation behavior under the indenter.

II. EXPERIMENTAL

The samples were made using a sinter forging tech-nique.[10] In brief: Ti, SiC and graphite powders were mixed, milled, cold pressed, and sintered in Ar at 1450 °C for 8 h. The sintered porous billets were hot pressed under plane strain conditions in a graphite die at 1600 °C under an axial stress of 42 MPa for 24 h. The resulting sample had large, plate-like grains with diameters of 1 to 2 mm and thicknesses of the order of 200 μm. The samples were cut with a diamond saw, mounted, and polished with a 0.06 μm colloidal silica suspension, and lastly etched and polished one more time to relieve any surface mechanical damage accumulated during polishing.

The orientations of the grains were confirmed using orientation imaging microscopy (OIM). Orientation im-aging microscopy is a relatively new technique using electron back-scattered diffraction to determine the crys-tallographic structure of polycrystalline specimens, such as crystallographic texture and orientation of individual grains with respect to the sample surface.[15–17] Using OIM, various grains with orientations with c axis close to 0° and 90° with respect to the indentation direction were selected. More details can be found in Ref. 17.

Load cycle indentations were carried out using a na-noindenter (MTS XP System, Corporation, Oak Ridge, TN) with a 13.5-μm-radius spherical diamond tip. The tip was calibrated with standard amorphous silica and sapphire samples. The tests were carried out—under load control at loading rates between 0.5 mN/s and 8 mN/s—to peak loads of 5, 10, 20, 100, 200, and 500 mN, in two orthogonal orientations: 0° and 90° to the c axis, respec-tively (i.e., parallel and normal to the c axis). To discount any experimental artifacts, similar tests were carried out in fused silica and sapphire at the above loads for com-parison. Two types of tests were carried out: first, regular indentation tests under load control, loaded to the termi-nal load, held there for 15 s, and unloaded. In the second type, repeated indentations were carried out up to 5 times on the same location to study the effects of cycling.

The load–displacement curves were converted into stress–strain curves.[8,18–25] For details on the technique and the assumptions made in this work, see Appendix.

III. RESULTS

The response of Ti$_3$SiC$_2$ to indentation loadings can be characterized by three regimes: (i) linear elastic, (ii) hys-teretic, reversible but without microscopic damage, fol-lowed by, at higher stresses, and (iii) plastic with damage (i.e., microcracking/delaminations). As noted above,

Ti_3SiC_2 is strongly anisotropic in its plastic properties, and therefore in the following we describe separately the behavior when the grains are indented parallel and normal to the c axis. (Where appropriate a schematic of the relationship between the loading direction and the basal planes is shown in the figures for each test as a schematic inset.)

For reasons that are not entirely clear, the stress–strain curves at strains less than approximately 0.03 were noisy and irreproducible and were omitted. Instead, in that range a straight line was drawn through the origin assuming a modulus[2,3] of 320 GPa, and Eq. (A6) in the Appendix. All other dashed lines shown in all figures, whether on re-loading or unloading, were drawn parallel to this original dashed line.

A. Loading normal to the c axis

When the load was applied normal to the c axis, (i.e., edge-on to the basal planes), at the highest peak loads (≈500 mN) delamination and/or cracks resulted in distinct pop-ins in the load displacement curves [Fig. 1(a)]. The load at which the pop-ins occurred was somewhat stochastic, but most pop-ins occurred at loads over

approximately 300 mN. Whenever pop-ins were recorded, the indents were clearly visible [see SEM micrograph in Fig. 1(a)]. A good correlation was found between the extent (in nm) of the pop-ins and the size of the cracks measured in the SEM, confirming their relationship. Interestingly, in two cases, no pop-ins were observed even at 500 mN [Fig. 1(a)].

Generally, at loads less than approximately 300 mN, no pop-ins were observed, and typical results obtained from multiple repeat indentations on the same location at 200 mN are shown in Fig. (1b). In this regime the first loop is slightly open indicating a small (50 to 100 nm) residual permanent deformation. However, the next four indentations, on the same location, result in fully reversible, almost indistinguishable, hysteresis loops [Fig. 1(b)]. The areas encompassed by the repeat loops are always smaller than the first loop [Fig. 1(b)], clearly indicating hardening.

The corresponding stress strain curves for the loops shown in Fig. 1(b) are shown in Fig. 1(c). Not surprising, the first loop is open, but the next four loops are indistinguishable from each other and, most important, are
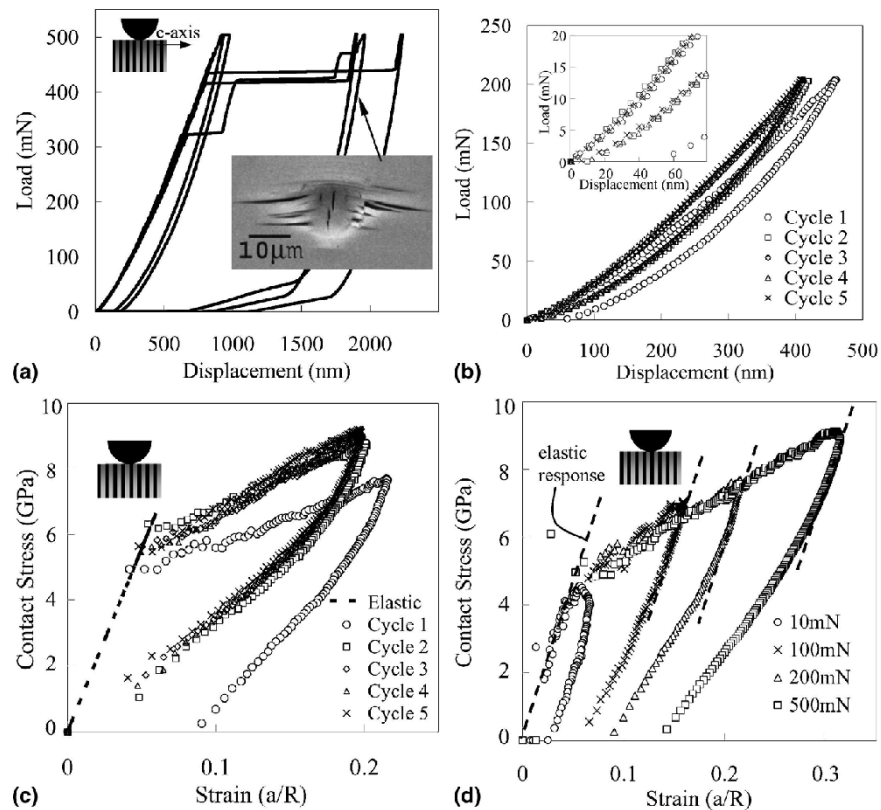

FIG. 1. (a) Typical load versus depth-of-indentation response of a Ti_3SiC_2 surface for which the loading direction is normal to the c axis. (Sketch on left in this and most other figures shows the indenter/c-axis arrangement). Five curves are shown; three show extensive pop-ins that resulted in delamination cracks shown in the central SEM micrograph; the other two did not delaminate and no trace of the indentation was found in the SEM. Note stochastic nature of load at which the pop-ins occur. (b) Same as (a), but for repeat indentations, in the same location, to a maximum load of 200 mN. Note first loop is open, but following 4 are closed. Inset expands the low load region. Major hardening occurs between the first and second cycles. (c) Contact stress versus strain for results shown in (b). Note full reversibility of repeat loops. (d) Contact stress versus strain for 4 different loads on four different locations. The inclined dashed lines were generated using Eq. A6, assuming a modulus of 320 GPa.

fully reversible as the extrapolation of the unloading curves all intersect the x axis at the origin. For the first cycle, a distinct back-extrapolated indentation yield point at approximately 4.5 GPa is observed [Fig. 1(c)]. (Note the stress computed is an average stress in a complicated stress state caused by the indenter geometry. Therefore, this yield point does not necessarily correspond to a yield point measured in simple compression tests. On the second and further cycles, this back-extrapolated indentation yield point increases to approximately 5.5 GPa (Fig. 1(c)]. Figure 1(d) shows the stress strain curves for 4 indentations on different locations at 10, 100, 200, and 500 mN. The reproducibility of the loading curves at the higher loads and that of the indentation yield points is noteworthy.

Note the 10 mN indentation loop in Fig. 1(d) yields an indentation yield point closer to 3.5 GPa, which is lower than the 4.5 GPa quoted above. It is well known in metal plasticity that the micro-yield point, where plastic deformation initiates first, can be significantly lower than the macroscopic yield point. The measurements shown here indicate that the same is probably true for Ti₃SiC₂ as well.

To study the response at low load levels in more detail, repeated nanoindentation measurements at 10 mN were performed. The corresponding stress–strain curves are shown in Fig. 2(a), where successive loops are shifted to the right for clarity. It is gratifying that the loading and unloading curves, for the five cycles, are parallel to each other and consistent with the assumed modulus of 320 GPa. Another interesting aspect of these results is that, in contradistinction to the results obtained at higher loads [Fig. 1(c)], the indentation yield point in these low load tests does not increase significantly with accumulated permanent deformation [compare cycles 2 and 4 in Fig. 2(a)].

Finally, despite stresses at the tip of the indenter of the order approximately 10 GPa and the repeat nature of the indentations, typically, in the absence of pop-ins, *no trace* of the indentations was found in a field-emission scanning electron microscopy (FESEM). In a few sporadic cases, a subtle patch was noted in the FESEM.

B. Loading parallel to the c axis

When the maximum load (500 mN) was applied parallel to the c axis, the propensity and especially the extent of pop-ins were greatly reduced [Fig. 3(a)] compared to when the load was applied parallel to the c axis [compare Figs. 1(a) and 3(a)]. In some cases there was a clear indication of selective slip of surface layers relative to bulk [see micrograph in Fig. 3(a)] that are not unlike the bunching up of a rug.

In general, the results obtained in this direction were less reproducible than the ones loaded in the orthogonal direction. The indentations in this direction sometimes had an extended penetration at low loads [e.g., Fig. 2(b)] and the results were thus quite stochastic. The differences between the repeat cycles, however, were much smaller. Possible reasons for this state of affairs are discussed below.

Typical load–displacement curves [Fig. 3(b)] obtained when loading to intermediate loads—100 mN—were similar to those loaded to higher loads. A few small pop-ins were observed, but the repeat cycles were almost superimposable [Fig. 3(b)]. The inset in Fig. 3(b) expands the low load area and indicates that the major hardening occurred between the first and second cycles, after which the rate of hardening diminished. The corresponding stress–strain curves are shown in Fig. 3(c) and are reminiscent of those shown in Fig. 2(a). The presence of a linear elastic region followed by a plastic region with a back-extrapolated indentation yield point of approximately 4 GPa is apparent. Here again the majority of the hardening occurred between the first and second cycles,
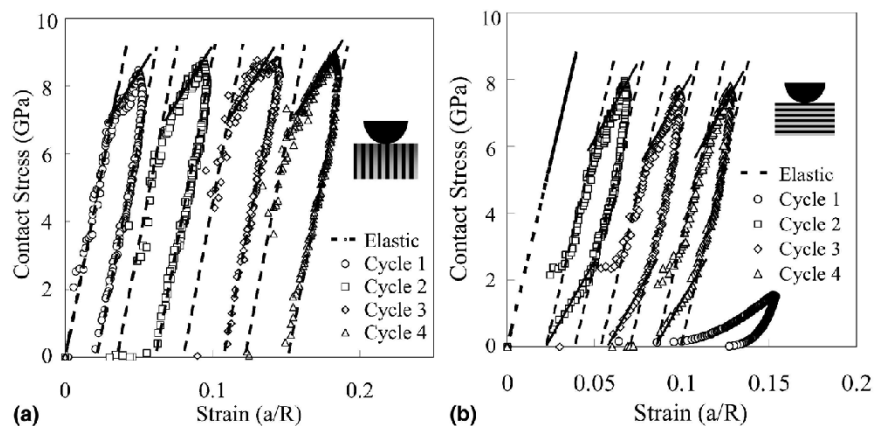
FIG. 2. Contact stress versus strain curves obtained when material was indented: (a) normal to the c axis up to 10 mN. Note increase in loop areas between first and second loops, but little change in yield points. (b) Parallel to the c axis up to 10 mN. First cycle is characterized by large deformations and low stresses. Second and subsequent cycles are almost identical in shape and size. In both figures, the cycles are shifted to the right for clarity; the inclined long dashed lines are generated using Eq. (A6), assuming a modulus of 320 GPa; the short inclined lines are guides to the eye showing the feeble dependence, if any, of yield points on total strain.
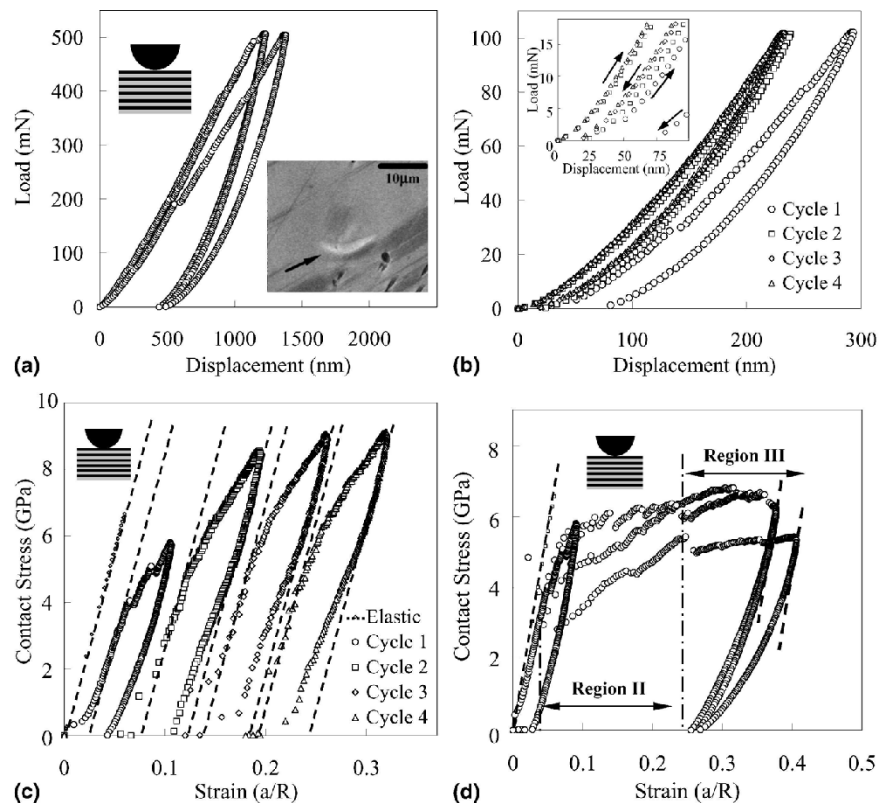
FIG. 3. (a) Typical load versus depth-of-indentation response of a Ti$_3$SiC$_2$ surface for which the c axis is normal to the surface. Three curves are shown for 3 different indent locations. In this direction, large pop-ins were not observed; instead features that resembled kinks in carpets shown in central SEM micrograph were observed. (b) Same as (a), but for repeat indentations, in the same location, to a maximum load of 100 mN. Inset expands the low load region. Major hardening occurs between the first and second loops. Note first loop is open, but following 4 appear closed. (c) Contact stress versus strain curves for results shown in (b). Note that in this case the loops are *not* reversible. In this figure the various cycles are shifted to the right for clarity. (d) Contact stress versus strain for 4 different loads on 4 different locations. Note stochastic nature of the yield points. Also note 3 regions: a linear elastic region; a region II where the hardening is rapid; and region III, where the hardening rate is lower. In both (c) and (d), the parallel inclined dashed lines were drawn assuming a modulus of 320 GPa and making use of Eq. (A6) in Appendix.

after which a saturation of sorts sets in. In contrast to the results shown in Fig. 1(c), here a small deformation is associated with each cycle.

The stress–strain curves for single indentations loaded to the maximum load [Fig. 3(a)] are shown in Fig. 3(d) and are characterized by three regimes: linear elastic, followed by a region where the hardening rate is relatively high [region II in Fig. 3(d)], followed, at the highest stresses by a region in which the hardening rate is much reduced [region III, Fig. 3(d)]. Note the variations in the yield points in this direction are significantly more scattered than the ones shown in Fig. 1(d).

As before, to study the response at low load levels in more detail, we carried out repeated indentations at 10 mN in this orientation as well. The resulting indentation stress–strain curves are shown in Fig. 2(b) and—if one ignores the first cycle, which is characterized by a large deformation at low stresses—the remaining curves are quite similar. Here again, the theoretical

straight line labeled elastic response in Fig. 2(b), fits the experimental results, provided the tail end of the data at low loads on loading are omitted. The unloading results also follow the same slope down to approximately 1 GPa, after which the data appears to skew to the left at roughly the same angle the loading curves tilt above the yield point.

C. Dissipated work

The area within the stress–strain loop is the energy dissipated during each cycle per unit volume, W_d. Figure 4 plots a log–log plot of W_d versus. σ as determined from the indentation stress–strain curves reported herein. Also included are the results obtained in our earlier work.[14] The agreement between the two sets of results is quite good considering the more than 6 orders of magnitude range in W_d covered by the data and the differences in the definitions and extraction of stress and strain between the uniaxial case[14] and this work.
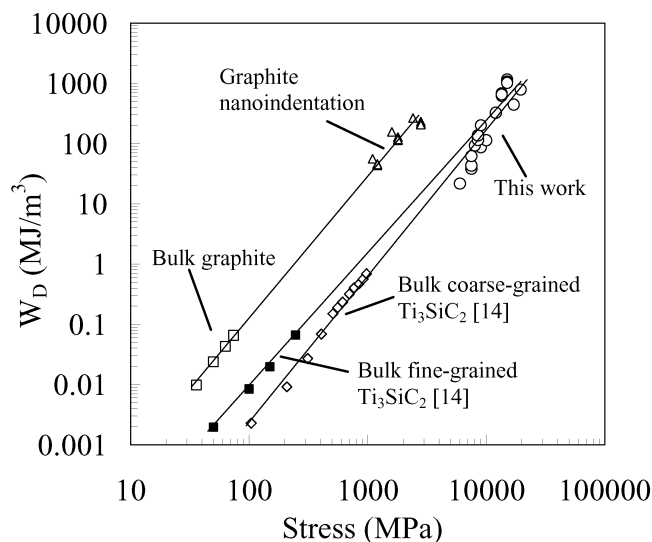
FIG. 4 Log-log plot of energy dissipated per cycle, W_d, versus maximum stress applied, σ for Ti_3SiC_2. The results in the lower left hand corner were obtained from simple compression results of bulk samples[14]. The ones in the upper right were obtained from the stress-strain curves generated in this work. The agreement is good despite the over 6 orders of magnitude range in W_d. The corresponding results for graphite are also shown.[31]

IV. DISCUSSION

As far as we are aware, the formation of near-fully reversible hysteresis loops, followed by hardening and fully reversible loops [e.g., Figs. 1(b) and 1(c)] has never been reported in any other *dense*, crystalline solid. Field and Swain,[21–23] Iwashita et al.,[25] and Sakai et al.[26] reported similar results but in glassy carbons.

For the most part, the dashed lines, based on a modulus of 320 GPa, fit very well for the initial portions of the loading and unloading curves for both orientations, confirming that the moduli along the *a* and *c* directions in Ti_3SiC_2 are not too different; a conclusion in line with recent ab initio calculations.[27] It is also in agreement with the mild anisotropy in thermal expansions along the *a* and *c* directions.[28] In that respect, Ti_3SiC_2 is quite different from other layered materials such as graphite or mica, that are both elastically and plastically anisotropic.

To understand and explain the majority of the results reported herein, it is essential to invoke the presence of three interrelated dislocation-based elements that appear in the solid as the stress is progressively increased: (i) incipient kink bands (IKBs); (ii) mobile walls (MWs) that form when the walls comprising the IKBs detach from each other; and (iii) immobile kink boundaries (KBs), which are thin areas in which the MWs have collapsed. The KBs are indistinguishable from high angle grain boundaries.

The strongest, and almost irrefutable, evidence for the presence of IKBs are the repeat cycles shown in Fig. 1(c). That the response is fully reversible is evident and that hardening has occurred between the first and second cycles is also indisputable. These two facts alone rule out phase transformations and/or microcracking. Furthermore, the fact that the energy dissipated is very large—of the order of >2 GJ/m³ (Fig. 4)—and reproducible is consistent with an interpretation in which not only are there numerous dislocations, but the latter can apparently glide *reversibly* over relatively large distances.

The hardening observed between the first and second cycles can be explained in the context of the KB model. During the first cycle, at low loads, IKBs are nucleated; at intermediate loads they split forming pairs of MWs that eventually collapse into KBs. According to Frank and Stroh,[29] the remote critical shear stress, τ_c, needed to render a subcritical kink band unstable (i.e., result in an IKB) is given by:

$$\tau_c \geq \sqrt{\frac{2bG^2\gamma\ln(1/\gamma)}{\alpha\pi^2(1-\nu)^2}} \quad , \qquad (1)$$

where ν is Poisson's ratio, G the shear modulus, α the size of the IKB domain, and b the Burgers vector. The most important ramification of Eq. (1), is that as α shrinks, the remote stresses required to initiate new IKBs increase accordingly. It is this reduction in domain size that explains the increase in yield point between the first and subsequent cycles [Fig. 1(c)]. Once a KB is formed, and as long as the stress is not increased above the initial stress, the only element that can nucleate is a fully reversible IKB. The small increase in yield points between the second and subsequent cycles [Fig. 1(c)] is probably a reflection of the fact that an equilibrium microstructure is not achieved after 5 cycles.

The idea of microstructure that ultimately reaches an equilibrium configuration—defined as one in which mobile dislocation walls are absent—for a given stress must clearly be invoked to explain the behavior of the material when loaded parallel to the c axis [Fig. 3(c)] and at low loads normal to the c axis [Fig. 2(a)]. In both cases, the loading and unloading curves are parallel and a permanent strain is recorded during each cycle. The results shown in Fig. 3(c) are remarkable and unique for two reasons:

(i) Despite the apparent hardening between the first and second, there is little doubt that W_d for the latter is greater than during the former. There is only one possible explanation to this observation: There are more mobile dislocations in the second cycle. As important, the fact that the areas of the later cycles are not a function of total strain [Fig. 3(c)] implies the density of these mobile dislocations also remains more or less constant.

(ii) The back-extrapolated nanoindentation yield points do not appear to increase despite the strain introduced during each cycle [Figs. 2(a) and 3(c)].

In context of our model, the simplest explanation is one in which a series of MWs radiate away from central IKB sources. Because the walls are parallel, they repel each other, but remain mobile, explaining both the source of the strain and the lack of hardening. Needless to add, at some point, the MWs collapse and form KBs, at which time the microstructure evolves toward equilibrium, ultimately leading to full reversibility. That an equilibrium microstructure does develop is best evidenced by the changes in shape of the stress–strain loops as the load in increased from 10 mN [Fig. 2(a)] to 200 mN [Fig. 1(c)]. At higher loads, the repeat loops are fully reversible. These comments notwithstanding, it is herby acknowledged that more work is needed especially at low loads and to higher number or cycles to better understand how the microstructure evolves. This is a topic of ongoing research.

The situation when the load is low (10 mN) and parallel to the c axis [Fig. 2(b)] is even more muddled because of the noise level and lack of reproducibility, especially of the first cycle. Here again more work is needed.

The results presented here are in complete agreement with our recent work[14] in which it was concluded that the formation of IKBs at room temperature—that gave way to KBs at higher temperatures—were responsible for the fully reversible hysteresis loops obtained in compression.[14] At room temperature, the failure stresses ($\approx$1 GPa for fine-grained samples) were insufficient to separate the IKB walls, and the response was fully reversible even for the first cycle. It is only at elevated temperatures that the walls of the IKBs separate and interact, resulting in smaller domains, which in turn account for the cyclic hardening observed at 1200 °C after cooling. In this work, the large stresses under the indenter and the confined nature of the deformation are sufficient to result in multiple KBs during the first cycle. In other words, the high stresses herein play the role of temperature in our previous work.

Based on the results shown in Fig. 4, it is reasonable to conclude that the processes occurring at room temperature during the compression of bulk Ti$_3$SiC$_2$ samples are the same as the ones occurring under the indenter. Such excellent agreement is consistent with our KB-based model. Note that the same good agreement between bulk and nanoindentation results is valid for graphite as well (Fig. 4).

The variability in response for samples loaded parallel to the c axis is not fully understood at this time. However, the presence of defects that can act as IKB nucleation sites and thus greatly lower the yield point cannot be discounted. The grains along the c direction are also much thinner than in the orthogonal direction,[10] and there is no easy way to determine the thickness of a given grain before indenting it. This could also have added to the experimental scatter observed. These comments notwithstanding, it is hereby acknowledged that more work is needed.

Direct evidence for micromechanical damage and KB formation under a large spherical indenter was published earlier.[8] Unfortunately, the results shown here and those reported in Ref. 8 cannot be compared, because in retrospect, it is now apparent that the deformation in the latter was not truly confined, which explains the strain-softening observed. In Ref. 8, the samples were split in two and re-glued together before loading.

In this paper, and despite some attempts, no direct evidence for the formation of KBs under the indentations is presented. Nevertheless, the key role KBs play in the deformation of Ti$_3$SiC$_2$—at all scales—is incontrovertible.[10–12,17,30]

Recently, direct transmission electron microscopy (TEM) evidence for the existence of KBs were observed when epitaxially grown thin films of Ti$_3$SiC$_2$ were nanoindented parallel to the c direction using a Berkovich indenter.[30] Direct TEM evidence for the presence of parallel dislocation walls and associated lattice rotations has also been reported.[12,30] Direct evidence for KBs was very recently obtained in single crystals of graphite[31] and mica.[32] Furthermore, scanning electron microscopy (SEM) micrographs of areas under the indenter unambiguously show a transformation of the single crystal into a multitude of much smaller crystals. Based on our recent work, there is thus little doubt that IKBs, MWs, and KBs play an important role in the deformation of both graphite, mica, and other layered silicates—and thus much of geology.[32]

It is also worth noting that reversible load–displacement curves have been reported in the literature in the indentation response of glassy carbons—composed of nanometer grains and 25–30% volume porosity.[21–23,25] The current interpretations invoke the reversible slip of carbon hexagonal network plane layers[21,26] or the reversible slip of dislocation networks, such as pile-ups at grain boundaries.[26] The data presented here raises the possibility that KBs might play a significant role in those materials as well. This merits further investigation.

The work described in this paper is of paramount importance for two main technological reasons. First, the fact that KBs can be initiated without apparent macroscopic damage raises several exciting possibilities. When this process is better understood, it could well lead to the development of processing methods for effectively refining a microstructure (possibly to nanolength scales) without associated damage. Second, Ti$_3$SiC$_2$, and by extension the other M$_{n+1}$AX$_n$ phases, can be loaded repeatedly without damage, while simultaneously dissipating

significant portions of the energy during each cycle. Based on this response, it is fair to assume that such surfaces would be highly resistant to fatigue damage. When taken together with the fact that the friction coefficients of the basal planes are ultralow,[33] the possibility of having high wear resistant surfaces that are very low friction is a tantalizing prospect. Furthermore, the prospect of exploring the more than 50 M$_{n+1}$AX$_n$ phases known to exist,[1] and innumerable combinations of solid solutions, is a wonderful one indeed, and one that should prove to be of technological and scientific importance and benefit. The absorption of energy during loading–unloading cycles could also in principle render the M$_{n+1}$AX$_n$ phases excellent surfaces for applications where vibration damping is desired; an important consideration for many micro-electro-mechanical systems applications.

V. CONCLUSIONS

Nanoindentations on Ti$_3$SiC$_2$ reveal three distinct regimes of mechanical response:

(1) Linear elastic response with an Youngs modulus of about 320 GPa, in directions parallel and normal to the c axis of the crystal.

(2) Hysteretic, reversible response without microscopic damage that is attributed to the formation of incipient kink bands, which with increasing load levels generate mobile dislocation walls, and eventually generate immobile kink bands. In this regime (up to about 200 mN loads), the first indentations often produce some permanent deformation that signifies production of kink bands. Repeated indentations in the same location to the same load level resulted in the development of an equilibrium microstructure that was evidenced by fully reversible load–displacement curves. There was clear evidence of hardening in these repeated indentations lending further support to the kinking models proposed here to explain the measurements.

(3) Plastic response with damage (i.e., microcracking/delaminations). It is important to note here that when the samples were loaded parallel to the c-axis, with the highest load possible, little to no damage was observed.

Back-extrapolated yield values were established. The indentation yield points in directions normal and parallel to the c axis were estimated to be about 4.5 GPa and 4 GPa, respectively.

Finally, a comparison of the energy dissipated per cycle per unit volume from the nanoindentation measurements showed remarkable agreement with the corresponding measurements from simple compression experiments when plotted against stress. This result suggests that the underlying mechanisms continue to be the same even at the high stress levels experienced in the nanoindentation experiments.

REFERENCES

1. M.W. Barsoum, The M$_{N+1}$AX$_N$ Phass: A new class of solids: Thermodynamically stable nanolaminates, Prog. Sol. State Chem., **28,** 201 (2000).
2. R. Pampuch, J. Lis, L. Stobierski, and M. Tymkiewicz, Solid combustion synthesis of Ti$_3$SiC$_2$, J. Eur. Ceram. Soc., **5,** 283 (1989).
3. M.W. Barsoum and T. El-Raghy, Synthesis and characterization of a remarkable ceramic: Ti$_3$SiC$_2$, J. Am. Ceram. Soc. **79,** 1953 (1996).
4. T. El-Raghy, M.W. Barsoum, A. Zavaliangos, and S.R. Kalidindi, Processing and mechanical properties of Ti$_3$SiC$_2$: II, effect of grain size and deformation temperature, J. Am. Ceram. Soc. **82,** 2855 (1999).
5. T. El-Raghy, A. Zavaliangos, M.W. Barsoum, and S.R. Kalidindi, Damage mechanisms around hardness indentations in Ti$_3$SiC$_2$, J. Am. Ceram. Soc. **80,** 513 (1997).
6. C.J. Gilbert, D.R. Bloyer, M.W. Barsoum, T. El-Raghy, A.P. Tomsia, and R.O. Ritchie, Fatigue-crack growth and fracture properties of coarse and fine-grained Ti$_3$SiC$_2$, Scr. Mater. **42,** 761 (2000).
7. M. Radovic, M.W. Barsoum, T. El-Raghy, and S. Wiederhorn, Tensile creep of fine-grained (3-5 μm) Ti$_3$SiC$_2$ in the 1000–1200 °C temperature range, Acta Mater. **49,** 4103 (2001).
8. I.M. Low, S.K. Lee, B. Lawn, and M.W. Barsoum, Contact damage accumulation in Ti$_3$SiC$_2$, J. Amer. Ceram. Soc. **81,** 225 (1998).
9. Y. Kuroda, I.M. Low, M.W. Barsoum, and T. El-Raghy, Indentation responses and damage characteristics of hot isostatically pressed Ti$_3$SiC$_2$, J. Aust. Ceram. Soc. **37,** 95 (2001).
10. M.W. Barsoum and T. El-Raghy, Room temperature ductile carbides, Met. Mater. Trans. **30 A,** 363 (1999).
11. L. Farber, I. Levin, and M.W. Barsoum, HRTEM study of a low-angle boundary in plastically deformed Ti$_3$SiC$_2$, Philos. Mag. Lett. **79,** 4103 (1999).
12. M.W. Barsoum, L. Farber, and T. El-Raghy, Dislocations, kink banks and room temperature plasticity of Ti$_3$SiC$_2$, Met. Mat. Trans. **30A,** 1727 (1999).
13. M.W. Barsoum, M. Radovic, P. Finkel, and T. El-Raghy, Ti$_3$SiC$_2$ and ice, Appl. Phys. Lett. **79,** 479 (2001).
14. M.W. Barsoum, T. Zhen, S. Kalidindi, M. Radovic, and A. Murugaiah, Fully reversible dislocation-based compression deformation of Ti$_3$SiC$_2$ to 1 GPa, Nat. Mater. **2,** 107 (2003).
15. B.L. Adams, Orientation imaging microscopy: Emerging and future applications, Ultramicroscopy **67,** 11 (1997).
16. D.P. Field, Recent advances in the application of orientation imaging, Ultramicroscopy **67,** 1 (1997).
17. B.J. Kooi, R.J. Poppen, N.J.M. Carvalho, J.Th.M. De Hosson, and M.W. Barsoum, Ti$_3$SiC$_2$: A damage tolerant ceramic studied with nano-indentations and transmission electron microscopy, Acta. Mater. **51,** 2859 (2003).
18. D. Tabor, *Hardness of Metals* (Clarendon Press, Oxford, U.K., 1951).
19. B.R. Lawn, N.P. Padture, H. Cai, and F. Guiberteau, Making ceramics "ductile", Science **263,** 1114 (1994).

20. F. Guiberteau, N.P. Padture, and B.R. Lawn, Effect of grain size on hertzian contact damage in alumina, J. Am. Ceram. Soc. **77,** 1825 (1994).

21. J.S. Field and M.V. Swain, The indentation characterization of the mechanical properties of various carbon materials: Glassy carbon, coke, and pyrolytic Graphite, Carbon **34,** 1357 (1996).

22. M.V. Swain and J.S. Field, Investigations of the mechanical properties of two glassy carbon materials using pointed indenters, Philos. Mag. A. **74,** 1085 (1996)

23. M.V. Swain, Mater. Sci. Eng. Mechanical property characterization of small volumes of brittle materials with spherical tipped indenters, **A253,** 160 (1998).

24. A.C. Fischer-Cripps, A review of analysis methods for sub-micron indentation testing, Vacuum **58,** 569 (2000).

25. N. Iwashita, M.V. Swain, J.S. Field, N. Ohta, and S. Bitoh, Elasto-plastic deformation of glass-like carbons heat-treated at different temperatures, Carbon **39,** 1525 (2001).

26. M. Sakai, Y. Nakano, and S. Shimizu, Elastoplastic indentation on heat-treated carbons, J. Am. Ceram. Soc. **85,** 1522 (2002).

27. B. Holm, R. Ahuja, and B. Johansson, Ab initio calculations of the mechanical properties of Ti₃SiC₂, Appl. Phys. Lett. **79,** 1450 (2001).

28. M.W. Barsoum, T. El-Raghy, C.J. Rawn, W.D. Porter, A. Payzant and, C. Hubbard, Thermal properties of Ti₃SiC₂, J. Phys. Chem. Solids **60,** 429 (1999).

29. F.C. Frank and A.N. Stroh, On the theory of kinking, Proc. Phys. Soc. **65,** 811 (1952).

30. J.M. Molina-Aldareguia, J. Emmerlich, J. Palmquist, U. Jansson, and L. Hultman, Kink formation around indents in laminated Ti₃SiC₂ thin films studied in the nanoscale, Scri. Mater. **49,** 155 (2003).

31. M.W. Barsoum, A. Murugaiah, S.R. Kalidindi, and Y. Gogotsi, Kink bands, nonlinear elasticity and nanoindentations in graphite, (accepted for publication in Carbon).

32. M.W. Barsoum, A. Murugaiah, S.R. Kalidindi, and T. Zhen, Kinking nonlinear elastic solids, nanoindentations and geology, (submitted to Physical Review Letters).

33. S. Myhra, J.W.B. Summers and E.H. Kisi, Ti₃SiC₂—A layered ceramic exhibiting ultra-low friction, Mater. Let. **39,** 6 (1999).

34. K.L. Johnson, *Indentation Contact Mechanics* (Cambridge University Press, Cambridge, 1985).

APPENDIX

According to Hertz for an elastic contact, applying a load of P using a spherical indenter of radius R results in a penetration depth, h_e given by:

$$h_e = \left(\frac{3P}{4E^*}\right)^{2/3} \left(\frac{1}{R}\right)^{1/3} \quad , \tag{A1}$$

where h_e is the penetration depth of the indenter relative to the original surface. E^* is the reduced modulus given by:

$$\frac{1}{E^*} = \frac{1 - \nu_s^2}{E_s} + \frac{1 - \nu_i^2}{E_i} \quad , \tag{A2}$$

where ν is Poisson's ratio, and the subscripts s and i refer to the specimen and the indenter, respectively.
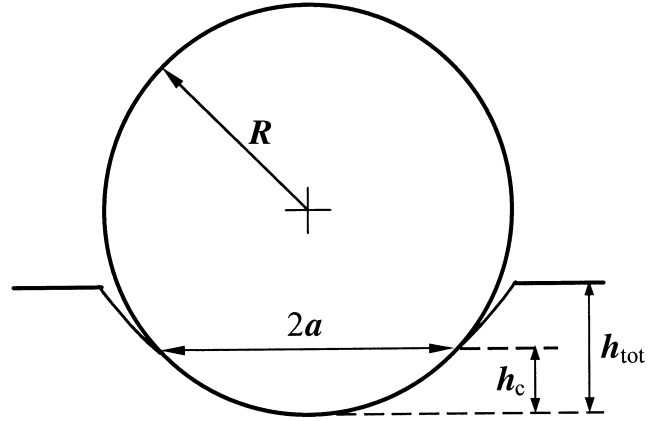

FIG. A1. Schematic of indentation with a spherical indenter, showing the actual area of contact, at small indentation depths ($h_c \ll R$).

Geometrically, the actual contact diameter $2a$ is related to h_c (Fig. A1) by:[24]

$$a = \sqrt{2R\, h_c}, \; h_c \ll R \quad , \tag{A3}$$

where h_c is the depth at which the indenter and surface are no longer conformal. Note that Eq. (6) in Ref. 21 and Eq. (4) in Ref. 25 are incorrect; a factor of 2 is missing.

Assuming that in the purely *elastic* regime[24,25,34]:

$$h_c \sim h_e/2 \quad , \tag{A4}$$

implies

$$h_e = a^2/R \quad . \tag{A5}$$

Note this equation implies that in the elastic regime $(a/R) = h_e/a$.

Using equation (A5) to eliminate h_e from Eq. (A1) yields the sought after result:

$$\frac{P}{\pi a^2} = \frac{4}{3\pi} E^* \left(\frac{a}{R}\right) \quad . \tag{A6}$$

For Ti₃SiC₂, $\nu = 0.2$ and its Young's modulus is 320 GPa. The corresponding values for the diamond indenter are $\nu = 0.07$ and 1170 GPa. As noted above, the excellent agreement between most of the loading and unloading curves and the lines generated assuming a modulus of 320 GPa confirms the validity of this technique. As important the control experiments carried out on silica (up to 200 mN) yielded stress–strain curves that were linear, and fully reversible and exhibited no hysteresis. The moduli measured from the control experiments were within 5% of the accepted value for the moduli of fused SiO₂; viz. 70 GPa.

Beyond the "yield point", the deformation is elasto-plastic and h_c in this regime is usually assumed to be[25]

$$h_c = h_{tot} - h_e/2 \qquad (A7)$$

where h$_{tot}$ is the measured total penetration (elasto-plastic) from experiment and h_e is computed from Eq. A1 assuming purely elastic contact.

In this paper, the hysteretic energy loss per unit volume, W_d, was determined from the computed indentation stress–strain curves. The effective volume over which the hysteretic energy loss is dissipated under the indenter can be estimated by dividing hysteretic energy loss computed directly from the load–displacement curves by W_d. The energy may be assumed to be dissipated in a cylinder of radius a and depth h_{eff} under the indenter. For the data presented in this study, h_{eff} was found to be around 1.5a, a value that is quite reasonable and validates the computation of W_d from the indentation stress–strain curves.

J. Mater. Res., Vol. 19, No. 7, Jul 2004

2203